Infrared Physics and Technology 93 (2018) 362–374

Contents lists available at ScienceDirect

Infrared Physics & Technology

journal homepage: www.elsevier.com/locate/infrared

Regular article

A robust framework for quality enhancement of aerial remote sensing images

Karuna Kumari Eerapu[a], Devikalyan Das[b], Shilpa Suresh[a], Shyam Lal[a,*], A.V. Narasimhadhan[a]

[a] Department of Electronics and Communication Engineering, National Institute of Technology Karnataka, Surathkal, Mangaluru 575025, Karnataka, India
[b] Department of Electronics and Telecommunication Engineering, Veer Surendra Sai University of Technology, Burla, Sambalpur 768018, Odisha, India

ARTICLE INFO

Keywords:
Aerial images
Contrast enhancement
PSO algorithm, Framework

ABSTRACT

This paper proposes a robust framework for quality restoration of remotely sensed aerial images. Proposed framework works in three steps: (1) Efficient color balancing and saturation adjustment, (2) Efficient color restoration, (3) Modified contrast enhancement using particle swarm optimization (PSO). In order to show the robustness, step-wise results of proposed framework is illustrated. Several aerial images from two publically available datasets are tested to support the robustness of the proposed framework over existing image quality restoration methods. The experimental results of proposed framework and other existing quality restoration methods are compared in terms of NIQMC, BIQME, MICHELSON, DE, EME and PIXDIST along with visual experimental results. Based on experimental results conducted on several aerial images suggest that the proposed framework is outperform over existing quality restoration methods.

1. Introduction

Satellite images are commonly have been used in the diverse fields like space, geosciences and etc for various applications [1,2]. Other than using satellite images for surveillance application, aerial remote sensing images captured from aero-planes are also important source of information for surveillance [3,4]. In addition to surveillance application, aerial remote sensing images are also used extensively in many trip and mapping software packages like Google Earth and Microsoft Virtual Earth. These software packages provide geospatial information of the earth surface [5]. Unfortunately, aerial remote sensing images still suffer from the atmospheric degradation source as those satellite counterparts [5]. The reason for selecting aerial remote sensing images because satellite remote sensing images are more sensitive to atmospheric effects as compared with aerial remote sensing images [6]. The effects of atmosphere on aerial images are even negligible in the good weather condition [6]. Another reason, aerial images have very high spatial resolution and high geometric fidelity [6]. In the literature, the histogram equalization method is used as basic approach for image enhancement because of its simple implementation but this method always gives over enhanced result [7–11]. The image enhancements by the transform domain methods are mainly focused on enhancement of high frequency sub-band coefficients [12–14]. But, these methods are not suitable for aerial or satellite remote sensing images. The recent linking models based method often not suitable for aerial images because of over smoothing which provides the loss of information in the images [15]. In [16], authors developed method based on Non-local approach for enhancement of satellite images but fails for color images.

In the literature last one decade, In addition to the conventional methods, authors also developed image enhancement methods based several optimization algorithms. In this filed, Genetic algorithm (GA) is the first and foremost method for image enhancement. In [17,18], authors developed Genetic Optimization algorithm based method for of satellite images but it is computational complex than conventional methods. In [19], authors proposed automatic method using PSO algorithm for enhancement of images. In this method, PSO algorithm is used to enhance the image details by properly tuning parameters of algorithm by maximizing their defined objective function. This method was computationally less complex compared than GA based enhancement method. In [20,21], authors also proposed automatic method using PSO algorithm for enhancement of images. In this method, authors claim that their methods outperform GA based enhancement method.

In [22], authors proposed Multi objective PSO (MPSO) based method for contrast enhancement of gray scale images. In this method, authors have considered discrete entropy as first objective function which main objective is to maximization it and gamma correction as a second objective function for intensity preservation. Authors claim that

* Corresponding author.
E-mail address: shyam.mtec@gmail.com (S. Lal).

https://doi.org/10.1016/j.infrared.2018.08.014
Received 18 January 2018; Received in revised form 6 August 2018; Accepted 12 August 2018
Available online 16 August 2018
1350-4495/

their method provides better experimental results for gray scale images but also demonstrated discrepancies in the output images. In [23], authors proposed new enhancement method for contrast enhancement for images. In this method, authors have used Otsu's method for segmenting the histogram of original image into two sub-bands and equalizing both of them independently through optimized weighing constraints using PSO algorithm. This technique was less stable and computationally complex than other existing methods. Later in the literature, authors proposed methods based on hybridization of meta-heuristics optimization algorithms for contrast enhancement of images [24,25]. Experimental results of these methods are better but are computationally complex. In [26], authors proposed hybrid method by combining PSO with Negative Selection Algorithm (NSA) for enhancement of images [26]. In [27], authors proposed modified differentia evolution (MDE) based algorithm for contrast enhancement of satellite images. The simulation results were promising but it is computationally complex method.

Most of the above mentioned image restoration methods results in redundant artifacts on various remote sensing image datasets. In order to solve problems of above described image restoration methods, a robust framework is proposed for quality restoration of remotely sensed aerial images. Proposed framework works in three steps: (1) Efficient color balancing and saturation adjustment, (2) Efficient color restoration, (3) Modified contrast enhancement using PSO algorithm. The PSO algorithm was proposed by Kennedy and Eberhart in 1995 [28]. It was based on the swarming behavior such as fish and bird schooling in nature [29]. PSO algorithm mainly consists of mutation and selection phases. In PSO algorithm, there is no crossover phase, which means it provides a high mobility in particles with a high degree of exploration [29]. The main advantage of PSO algorithm is that it helps to speed up the convergence rate by drawing towards the current best, but at the same time PSO algorithm may lead to premature convergence [29]. The other quality restoration methods developed by various researchers for remote sensing image processing applications [30–39]. The main research contributions of this paper are given as follows:

- Modified Contrast Enhancement method using PSO algorithm is proposed for remotely sensed aerial images.
- A robust framework is proposed for quality enhancement of remotely sensed aerial images.
- Contribution to state-of-the-art contrast enhancement method for remotely sensed aerial images.

The structure of the manuscript is organized as follows. Section 2 gives detailed analysis of the proposed framework. Section 3 gives experimental results of proposed framework. Section 4 gives conclusion and future scopes of the manuscript.

2. Proposed framework

Design, implementation and analysis of the proposed framework are presented in this section. The proposed framework is delineated into three steps: (1) Efficient color balancing and saturation adjustment, (2) Efficient color restoration, (3) Modified contrast enhancement using PSO algorithm.

2.1. Efficient color balancing and saturation adjustment

A RGB aerial remote sensing image I is given as input with red (R), green (G), and blue (B) as it's channels and then It is normalized between 0 and 1 which is depicted below

$$S(i,j) = \{R(i,j),\ G(i.j),\ B(i,j)\} \in [0,\ 1] \tag{1}$$

where (i, j) denotes the pixel indices and $[0,\ 1]$ is the range of normalized magnitudes. The indices may be removed henceforth as it is understood from the context.

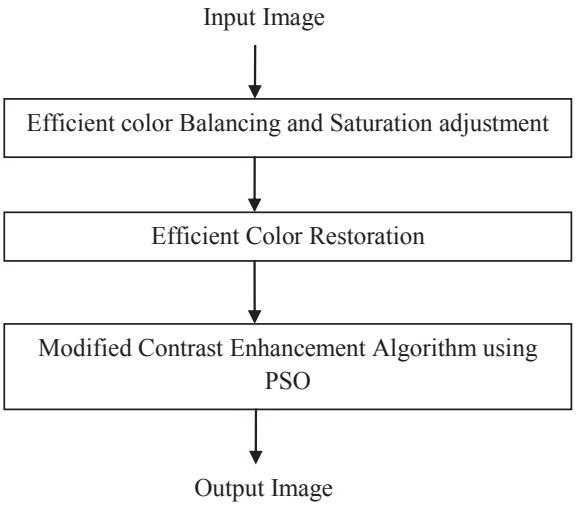

Fig. 1. Schematic representation of proposed framework.

According to grey-world assumption, the averaged image color is grey thereby eliminating color cast. For this assumption to hold there should be exponential alignment of the mean color values of the channels [3]. Moreover the use of exponent assures that all pixel values are within the prescribed range $[0,\ 1]$. First we calculated the minimum value of mean brightness for each input color channel [3] and is given by

$$S_{\mathrm{M}} = \min_{C}\left\{\frac{1}{N}\sum_{W,H} S^{C}\right\} \tag{2}$$

Where S^C denotes the pixel color magnitude for $C \in \{R,\ G,\ B\}$ and N depicts the total number of pixels which is actually the product of width (W) by height (H) of the input image, that is $N = W \times H$. The summation is performed for all three color components for all pixels.

The average values belonging to each channel are defined as

$$S_{\mathrm{M}}^{C} = \frac{1}{N}\sum_{W,H} S^{C} \tag{3}$$

Then, there is further alignment of each color channel to the mean image brightness and this is done by each pixel raised to an exponent [3]. It is given by

$$\kappa^{C} = \frac{\log(S_{\mathrm{M}})}{\log(S_{\mathrm{M}}^{C})} \tag{4}$$

where κ^Cdenotes the exponent for each individual color.

Removal of color cast is followed by saturation adjustment of image [3]. This is impelled by scrutinizing the definition of color saturation (CS) in both hue saturation intensity (HSI) and hue saturation value (HSV) color spaces and is given by

$$CS_{HSI} = 1 - \frac{3 \times \min\{R,\ G,\ B\}}{R + G + B} \tag{5}$$

$$CS_{HSV} = 1 - \frac{\min\{R,\ G,\ B\}}{\max\{R,\ G,\ B\}} \tag{6}$$

From here it can be easily deduced that saturation can be enhanced by compressing $\min\{R,\ G,\ B\}$ or amplifying $\cdot$. So our saturation adjustment comprises of two stages, which are described below.

First, there is global alignment of all the pixel magnitudes to cover $[0,\ 1]$ and is given by

$$S^{C} = \frac{S^{C} - \min_{C,WH}\{S\}}{\max_{C,WH}\{S\} - \min_{C,WH}\{S\}} \tag{7}$$

where $\min_{C,WH}\{S\}$ represents the minimum values calculated over all

Table 1
Step-wise enhancement results of proposed framework fort test Image 1.

Each stage	METRICES					
	NIQMC	BIQME	MICHELSON	DE	EME	PIXDIST
Input Image	3.8518	0.4056	0.0008	6.9188	7.4905	20.4753
Efficient color balancing and saturation adjustment (Step-1)	4.7004	0.5073	0.0219	7.2976	15.4438	21.9989
Efficient Color Restoration (Step-2)	5.2305	0.6105	0.1513	7.6709	25.2839	29.5533
Modified Contrast Enhancement using PSO (Step-3)	**5.4136**	**0.6456**	**0.3817**	**7.8024**	**55.0252**	**33.2337**

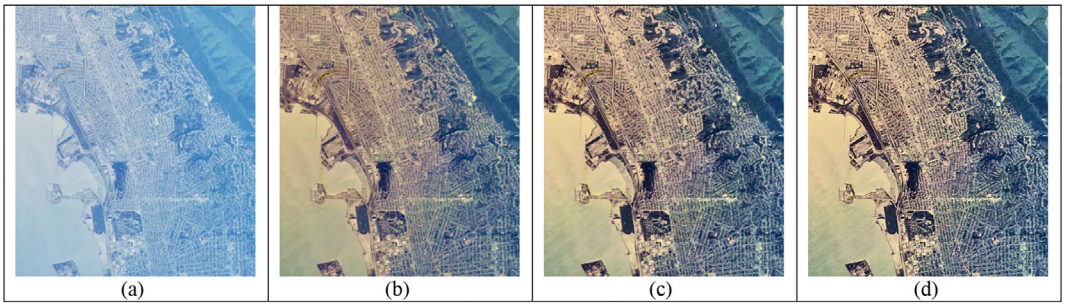

Fig. 2. Test image 1: (a) input (b) output of efficient color balancing and saturation adjustment (step-1), (c) Efficient Color Restoration (step-2), (d) Modified Contrast Enhancement using PSO(step-3).

Table 2
Parameters used in PSO algorithm.

Parameter name	Meaning	Default value
Population size (P)	Total number of candidate solution vectors initialized	30
No. of particles in the swarm (q)	Dimension of the problem / No. of parameters to be optimized	2
Total no. of generations (G)	No. of iterations	30
Inertia constant (n), acceleration constants (c_g, c_q)	Velocity update parameters	0.8, 1.7, 1.7
Initial velocity value ($v_{\min}$)	Lower boundary limit of particle velocity	0

color channels and pixels, $\max_{C,WH}\{S\}$ represents the maximum calculated over all color channels and pixels. After this process, at least one pixel with minimum color would be at zero and at least one pixel with maximum color would be at unity. Hence, as per the definition, there would be partial saturation enhancement of pixels.

Second, colors of each pixel would be sorted into three elements defined as minimum (β), middle (χ) and maximum (δ) which are color independent and satisfies the condition $\beta < \chi < \delta$. Further, for post-normalization we have defined a magnitude variable (μ) and is given by

$$\mu = \frac{\chi - \beta}{\delta - \beta} \tag{8}$$

This is the ratio of middle element to the min-max range. This is succeeded by a shift-and-scale process or in simpler term, compression and expansion of the minimum and maximum elements respectively depending on the parameter λ, $(0 < \lambda < 1)$ as depicted below,

$$\beta = (1-\lambda)\beta \tag{9}$$

$$\delta = \lambda + (1-\lambda)\delta \tag{10}$$

This operation is indeed needed for keeping the resultant elements within the range [0, 1].

The change in magnitudes of minimum and maximum element leads to color shift which is reduced by restoring original ratio of the middle element between the minimum and maximum elements and it is described below

$$\chi = \mu \times (\delta - \beta) + \beta \tag{11}$$

After this stage, the elements owing to their respective sorting index are remapped to their respective color channels and an image possessing improved saturation is obtained.

2.2. Efficient color restoration

The RGB saturated image from the prior step is processed further to overwhelm any sort of color violation. Here, a color restoration technique is employed which is basically an optimized search procedure based on an efficient search technique for computing and evaluating optimal parameters of the image, thereby enhancing the non-uniform illuminated regions [30]. This processed image is passed for a modified

Table 3
Average performance comparison of different techniques on aerial dataset1.

Algorithms	Metrices					
	NIQMC	BIQME	MICHELSON	DE	EME	PIXDIST
UMFKG	4.5450	0.5307	0.0588	7.5166	16.9545	28.2191
RHE-DCT	4.9611	0.5835	0.0642	7.4685	18.3882	25.3302
IFAIR	4.8026	0.5208	0.1237	7.2823	20.583	22.2855
LSCN	4.9651	0.6072	0.0964	7.4228	24.1191	24.2948
JEI	3.9011	0.4492	0.0013	7.0743	7.9222	20.2816
MDE	3.9587	0.4209	0.0009	6.9014	5.9131	22.4380
PROPOSED FRAMEWORK	**5.3429**	**0.6139**	**0.2537**	**7.7080**	**41.1225**	**30.4094**

Table 4
Average performance comparison of different techniques on aerial dataset2.

Algorithms	Metrices					
	NIQMC	BIQME	MICHELSON	DE	EME	PIXDIST
UMFKG	5.1461	0.5847	0.2617	7.4714	35.6825	25.2336
RHE-DCT	5.1419	0.5977	0.1169	7.458	22.1714	25.4332
IFAIR	4.8884	0.5676	0.1518	7.2917	22.7625	22.4501
LSCN	4.7361	0.5045	0.0759	7.2692	17.1117	21.8005
JEI	5.2434	0.5898	0.0659	7.6116	17.0655	28.5676
MDE	4.1863	0.4270	0.0158	7.0601	9.2292	20.6029
PROPOSED FRAMEWORK	**5.4479**	**0.6256**	**0.2756**	**7.7492**	**35.888**	**30.889**

contrast enhancement process.

2.3. Modified contrast enhancement using PSO algorithm

Following the enrichment of non-uniform illuminated regions, here a contrast enhancement process riveting on the image brightness is worked out. This process is a modified unsharp masking filter (UMF) [31]. The enhancement operation is carried out on the brightness space. For this the processed RGB image is converted to hue-saturation-value (HSV) space [32], where color is denoted by hue (H), the richness of the color is represented by saturation (S) and brightness is denoted by value (V). Here, the unsharp masking enhancement is performed on V-channel.

The operation of UMF is given as [33],

$$Z = V + s\,X \tag{12}$$

where Z is the filtered V-channel pixel, V is the given input V-channel pixel, $s$is the control factor deciding the strength of enhancement and $X$is the edge signal from the kernel. This is done using two steps.

2.3.1. Kernel design

The performance of UMF is largely dependent on the filter kernel used and the proper setting of gain factors. The improper setting of gain factor would make the output either under-enhanced or over-enhanced [33]. So, here a kernel ζ of 3×3 size is taken. The chosen kernel is used to extract local edge thereby giving thinner edges and improved sharpness in the enhanced image. The kernel given by

$$\zeta = \frac{1}{16} \times \begin{bmatrix} -a & -2 & -a \\ -2 & 12 & -2 \\ -a & -2 & -a \end{bmatrix} \tag{13}$$

and the constraint of kernel element is given by $a > 0$. The edge signal output from kernel is depicted by,

$$X = \zeta \otimes \Delta \tag{14}$$

where Δ, is the 3×3 neighborhood pixels positioned around pixel V.

The convolved output is scaled with control parameter s and is added to original image in order to obtain enhanced sharpness. Hence, to achieve desirable enhancement results, parameters a and s are required to be optimized. This is done using PSO algorithm.

2.3.2. Particle swarm optimization (PSO) algorithm

The PSO algorithm belongs to the class of meta-heuristic algorithm. It is inspired from the swarm behavior of living species in nature, such as fish and bird schooling, while searching for food [34,40–43]. The reason for choosing PSO algorithm for optimizing kernel parameters is that because it mainly consists of mutation and selection parameters. In PSO algorithm, there is no crossover phase, which means it provides high mobility in particles with a high degree of exploration [44]. Hence, it is suitable for finding optimal solutions to arduous optimization problems. The PSO algorithm has many advantages [45], which are: (1) Implementation of PSO algorithm is simple because it requires to set only few parameters (2) PSO algorithm is an effective in global search (3) PSO algorithm is insensitive to scaling of design variables, and (4) PSO algorithm is easily parallelized for simultaneous processing, it has propensity to result in a fast and early convergence in mid optimum points [45].

Here, in this optimization problem, the parameters are going to be optimized are kernel parameter element a, and parameter s. For this, a particle in PSO algorithm is encoded with these parameters and is given by

$$\mathrm{T} = [t_1\, t_2] = [\mathrm{a}\, s] \tag{15}$$

The swarm in PSO algorithm, consists of q particles, i.e., T_j where $j = 1, ..,q$ (q set as 2 in our designed problem). In the beginning, the particles are assigned its initial positions in a random manner, in the potential solution space. The population size (P) of the solution space is initialized as 30 and the maximum number of generations (G) is fixed as 30 [34]. Then, the particles are updated according to their defined objective function and during a number of time steps $i = 1,\ldots\ldots\ldots\ldots G$, they are guided to optimal solutions. The particles wander in the solution space and are attracted to global best solution T^g ascertained so far. The motion of the particle is controlled by its current best solution T_i^q . The new position of the particle is governed by its original position and velocity of motion [34]. The new velocity vector [34] is given in the Eq. (16).

$$v_{j,i+1} = n_j v_{j,i} + c_g\,(T_i^g - T_{j,i}) + c_q\,(T_{j,i}^q - T_{j,i}) \tag{16}$$

where velocity vector is denoted by$v$ and inertia constant is denoted as n which lies in the range ·. The acceleration constants are denoted as c_g and c_q, which are random numbers in [0, $c_{\max}$] and $c_{\max}$ is the maximum value taken between 1.7 and 2.0.

According to new velocity, the new position of the particle can be updated as given in the Eq. (17)

$$T_{j,i+1} = T_{j,i} + v_{j,i+1} \tag{17}$$

In this problem, $a > 0$ and $s > 0$, are the required constraints. Hence, both the constraints are satisfied by employing the given step

$$T_{j,i} \leftarrow |T_{j,i}| \tag{18}$$

The information content is determined by maximizing the objective function which is defined in the Eq. (19)

$$f_{obj} = \varepsilon \times \left(1 - \frac{\sigma}{W \times H}\right) \tag{19}$$

where ε denotes the entropy, σ denotes the number of over-ranged pixels. After maximizing this, output edge signal X is updated and after scaling with parameter s, it is superimposed onto the given V-channel image V and a higher contrast enhanced output v-channel image Z is obtained and it is again converted back to RGB channel to give the final output image. This framework is tested on a collection of different aerial remote sensing images.

2.4. Implementation of proposed framework

The schematic representation of proposed framework for quality

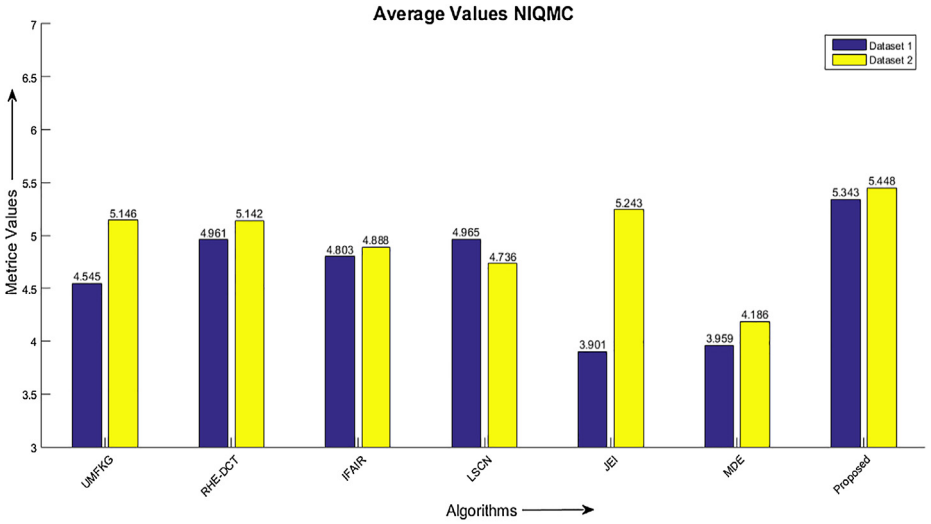

(a)

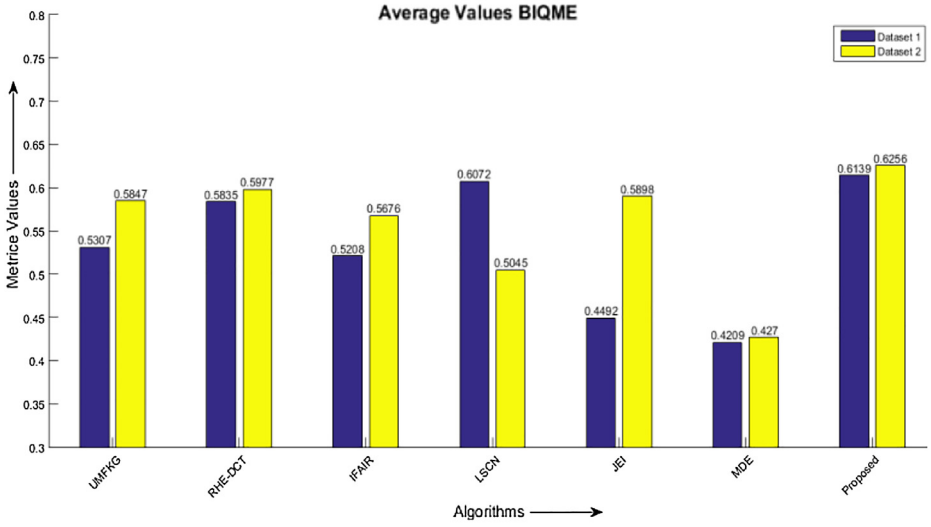

(b)

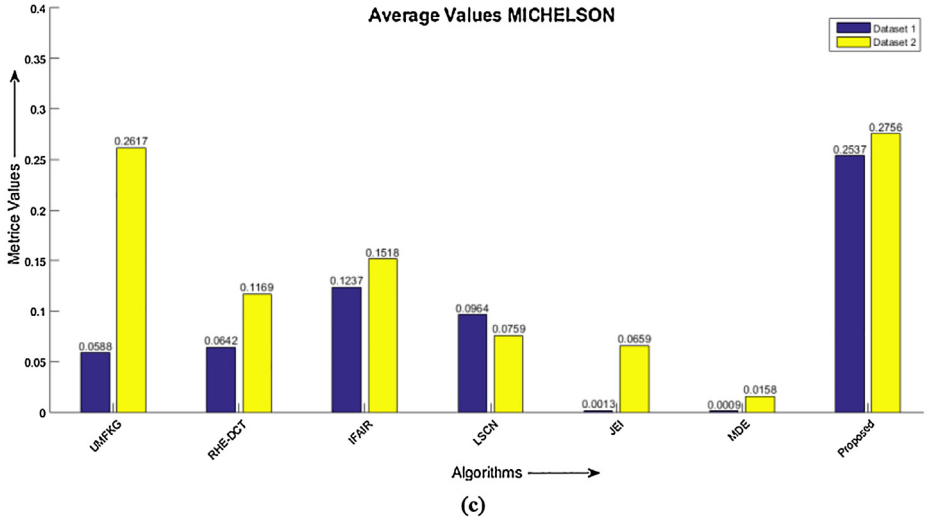

(c)

Fig. 3. Performancecomparison of difference through bar graph on aerial image dataset1 and dataset2.

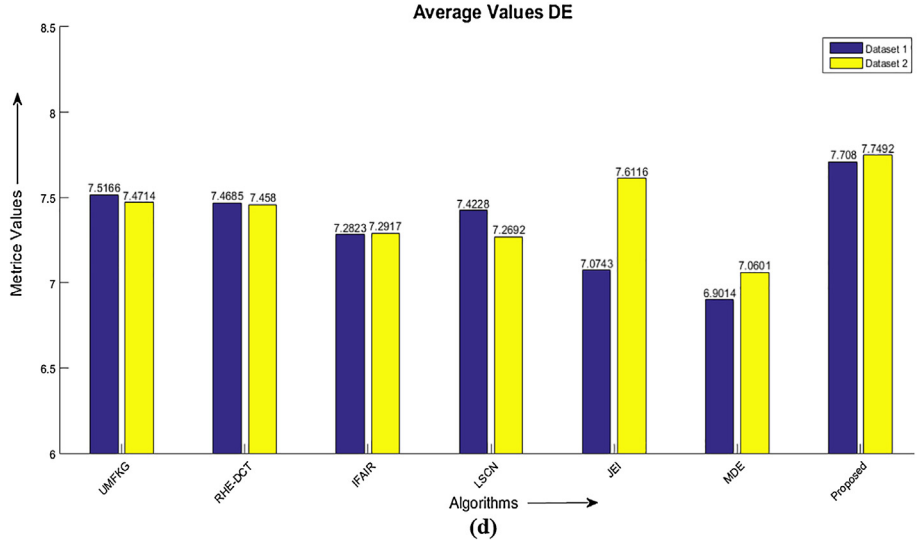

(d)

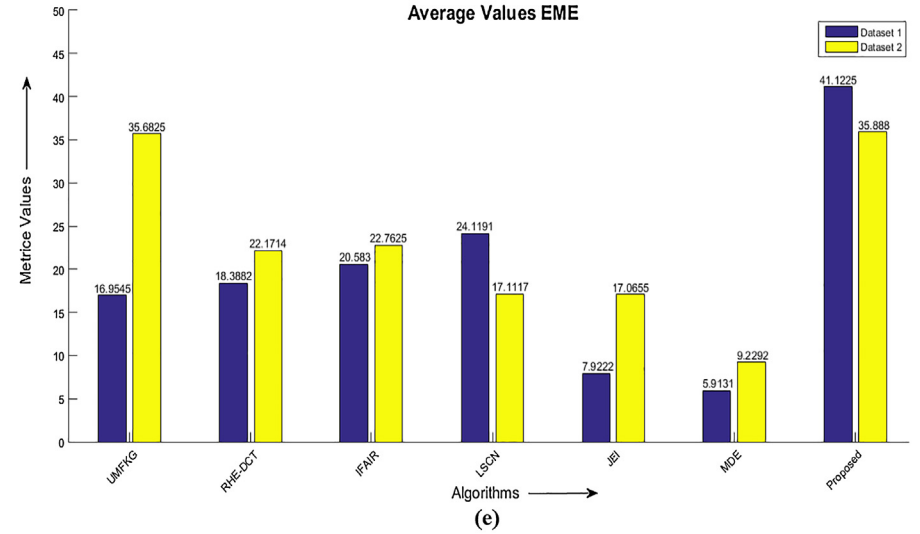

(e)

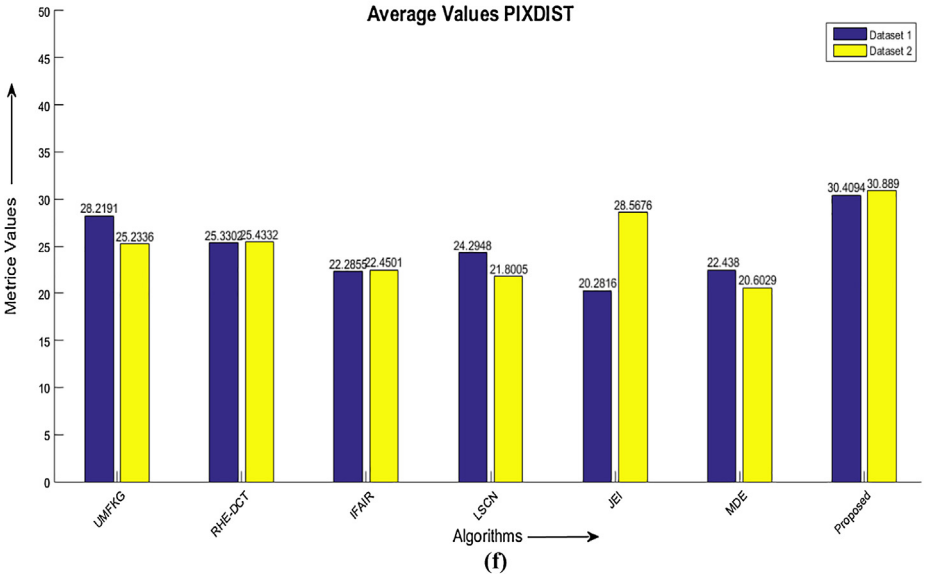

(f)

Fig. 3. (*continued*)

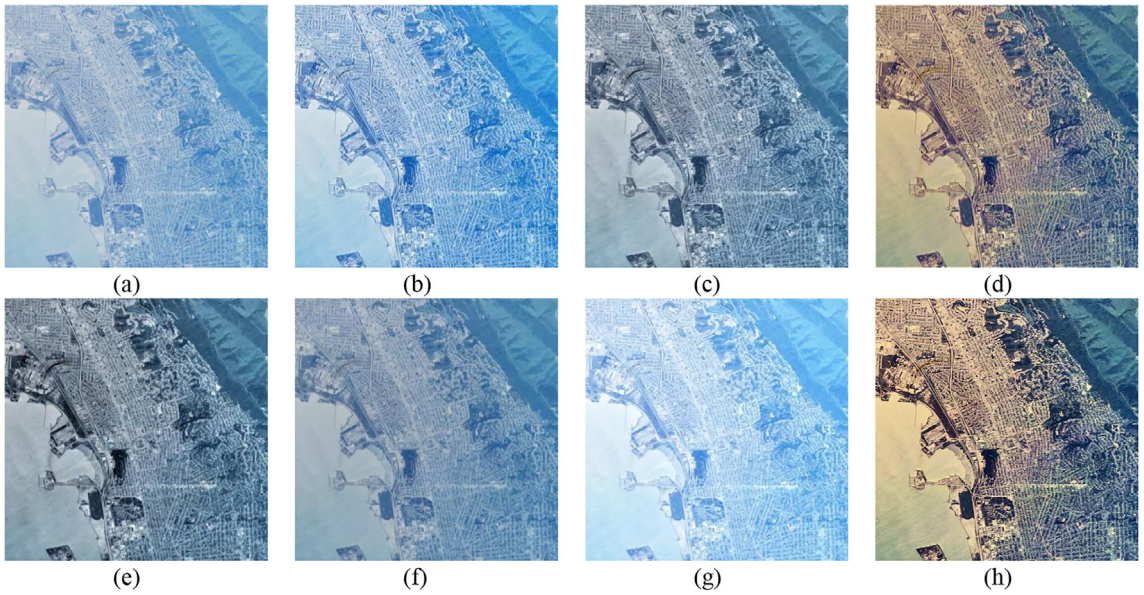

Fig. 4. Visual results of different quality restoration methods for aerial image 1. (a) Original image, (b) UMFKG, (c) RHE-DCT, (d) IFAIR. (e) LSCN, (f) JEI, (g) MDE, (h) PROPOSED FRAMEWORK.

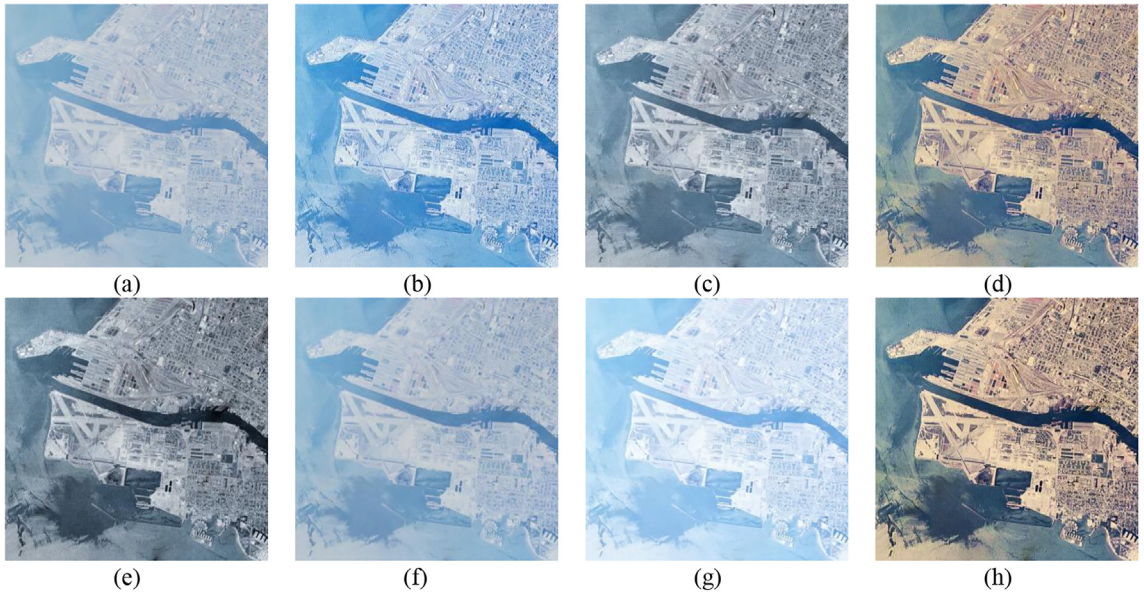

Fig. 5. Visual results of different quality restoration methods for aerial image 2. (a) Original image, (b) UMFKG, (c) RHE-DCT, (d) IFAI (e) LSCN, (f) JEI, (g) MDE, (h) PROPOSED FRAMEWORK.

restoration for aerial remote sensing images is shown in Fig. 1 and its implementation procedures are as follows:

Step 1: Efficient color balancing and saturation adjustment: In this step, a RGB aerial image is given as input and is normalized as given in Eq. (1). Then minimum value of mean brightness for each input color channel and the average values belonging to each channel are calculated as given in Eqs. (2) and (3). The gray–world color balance is given in Eq. (4) which is the exponent for alignment of each color channel. Then the image is stretched to align the color correction exponent. After this there will be saturation adjustment. First there will be partial saturation enhancement of the pixels as given in Eq. (7). Then colors of each pixel would be sorted into three elements defined as minimum, middle and maximum. These values are extracted as given in Eqs. (9), (10) and (11) respectively. Then the elements belonging to their respective sorting index are remapped to their respective color channels. An improved saturation adjusted image is obtained.

Step 2: Efficient Color Restoration: This step makes sure to get rid of any small color violation in the processed image before it is passed for contrast enhancement. This step maintains a fair degree of color constancy which described in the Section 2.

Step 3: Modified Contrast Enhancement using PSO: This is the last step which performs the contrast enhancement of the above processed image. First the processed RGB channel image is converted to HSV channel and the modified unsharp masking filter (UMF) is applied to this as given Eq. (12). To apply this, the filter kernel is given by Eq. (13) and the edge signal output obtained by the convolution of filter kernel and neighboring pixels matrix which is given in Eq. (14). The optimum value of the parameters in the kernel and the UMF are found out using PSO algorithm. Then encoding of the parameters is done and is given by Eq. (15). The new velocity vector and the position of the particle in the PSO are given in Eqs. (16) and (17). The objective function for maximizing the parameters is given in equation (19). The

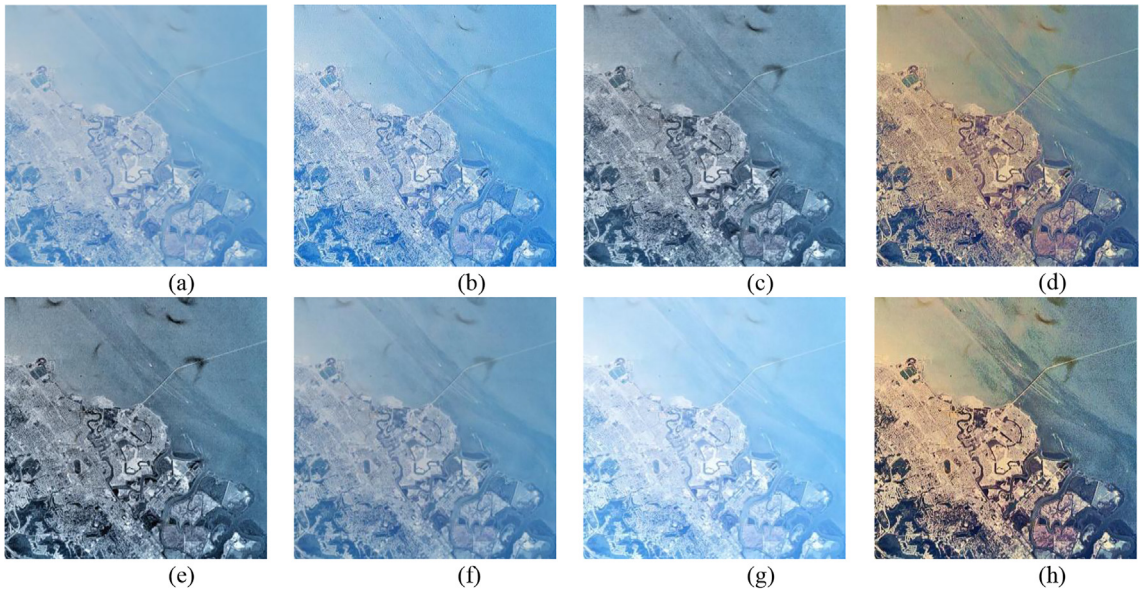

Fig. 6. Visual results of different quality restoration methods for aerial image 3. (a) Original image, (b) UMFKG, (c) RHE-DCT, (d) IFAIR, (e) LSCN, (f) JEI, (g) MDE, (h) PROPOSED FRAMEWORK.

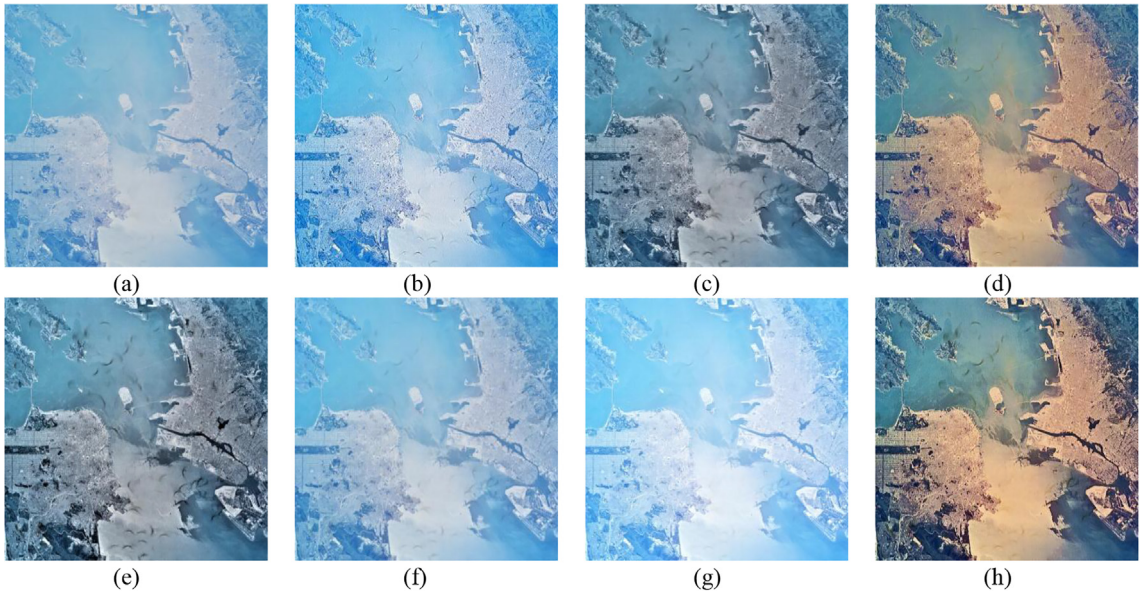

Fig. 7. Visual results of different quality restoration methods for aerial image 4. (a) Original image, (b) UMFKG, (c) RHE-DCT, (d) IFAIR, (e) LSCN, (f) JEI, (g) MDE, (h) PROPOSED FRAMEWORK.

updated values of the parameters are remapped to the V-channel of the image and the updated image is converted back to the RGB channel and it is the final output.

2.5. Illustration of proposed quality restoration framework

The proposed framework is divided into three major stages as discussed earlier. Quantitative results of each stage have been evaluated using the different image quality metrics (IQM) such as No-Reference Image Quality Metric for Contrast distortion (NIQMC) [46], Blind Image Quality Measure of Enhanced images (BIQME) [47], Michelson Contrast (MICHELSON) [48], Discrete Entropy (DE) [49,50], measure of enhancement (EME) [51] and Pixel distance (PIXDIST) [52] which are given in Table 1 for Image 1. Higher its value better is the quality restoration method. Visual enhancement results of each stage have been evaluated and are presented in Fig. 2.

3. Experimental results and discussion

Our proposed framework is tested and validated against a number of existing image quality restoration mehods on remotely sensed aerial image datasets. The image quality restoration methods included for simulation and experimental results comparison are UMFKG [31], RHE-DCT [16], IFAIR [3], LSCN [15], a method of JEI [30] and MDE algorithm [27].

3.1. Parameter setting

The values of the different parameters used in benchmarks image quality restoration methods are selected from their respective research papers. The different simulation parameters used in the proposed framework are derived by its working form and it is given in Table 2.

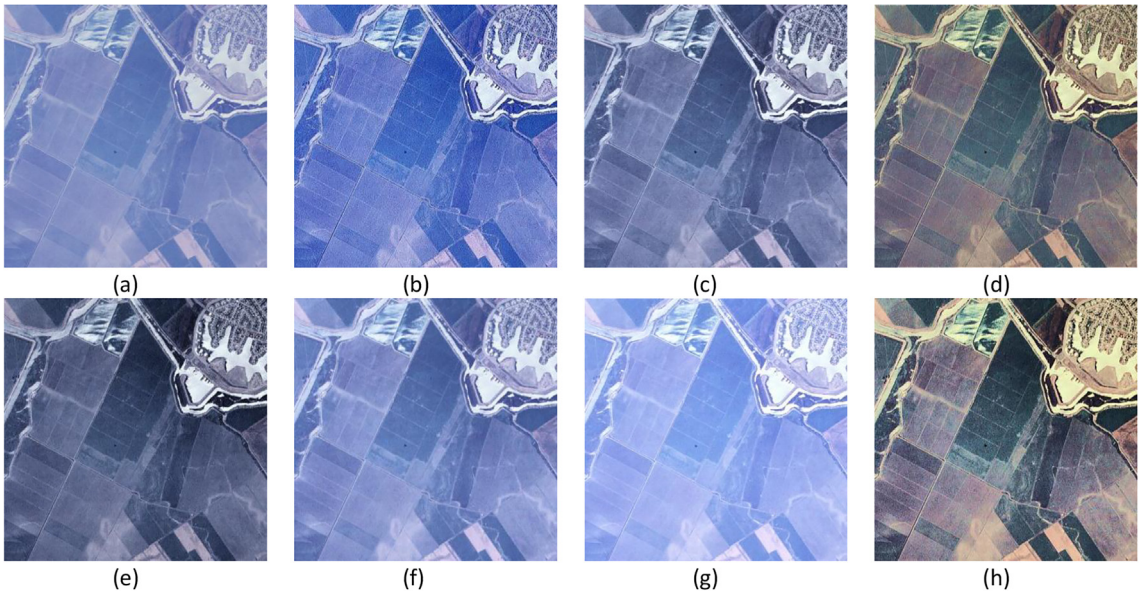

Fig. 8. Visual results of different quality restoration methods for aerial image 5. (a) Original image, (b) UMFKG, (c) RHE-DCT, (d) IFAIR, (e) LSCN, (f) JEI, (g) MDE, (h) PROPOSED FRAMEWORK.

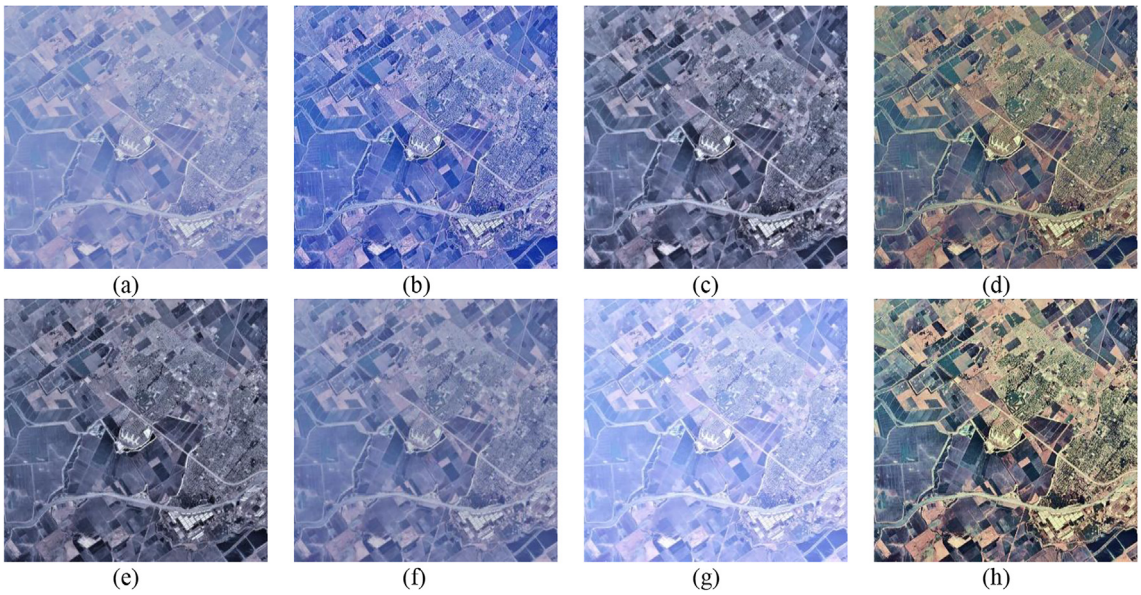

Fig. 9. Visual results of different quality restoration methods for aerial image 6. (a) Original image, (b) UMFKG, (c) RHE-DCT, (d) IFAIR, (e) LSCN, (f) JEI, (g) MDE, (h) PROPOSED FRAMEWORK.

3.2. Aerial remote sensing image datasets

In the simulation, the different test aerial remote sensing images were used from dataset1 and dataset2. These aerial datasets were procured from USC-SIPI Image database (source of dataset1: http://sipi.usc.edu/database/database.php?volume=aerials) and SZTAKI air change benchmark set (source of dataset2: http://web.eee.sztaki.hu/remotesensing/airchange_benchmark.html) [38,53]. First dataset contains total 37 aerial remote sensing images which were originally stored in the TIFF color format. In this dataset, twelve aerial images were 512x512 and twenty-five aerial images were 1024x1024. Second dataset contain total 12 aerial change detection remote sensing image which were originally stored in the BMP color format and each aerial image were size of 952 × 640.

3.3. Result analysis

In order to the simulation and experimental results assessment, performance evaluation and visual results comparison of proposed framework with other image quality restoration methods on different aerial image datasets is presented. The proposed framework and other existing image quality restoration methods are tested on 49 aerial remote sensing images from the above mentioned databases, but visual results of only 10 aerial images are presented in this manuscript. The numerical performance comparison of different image quality restoration methods is presented in terms of image quality metrics such as NIQMC [46], BIQME [47], MICHELSON [48], DE [49,50], EME [51] and PIXDIST [52]. Higher its numerical value better is the quality restoration method. Table 3 and Table 4 depict the average value of evaluated quality metric values for all the image quality restoration methods compared on aerial image dataset1 and dataset2. From the

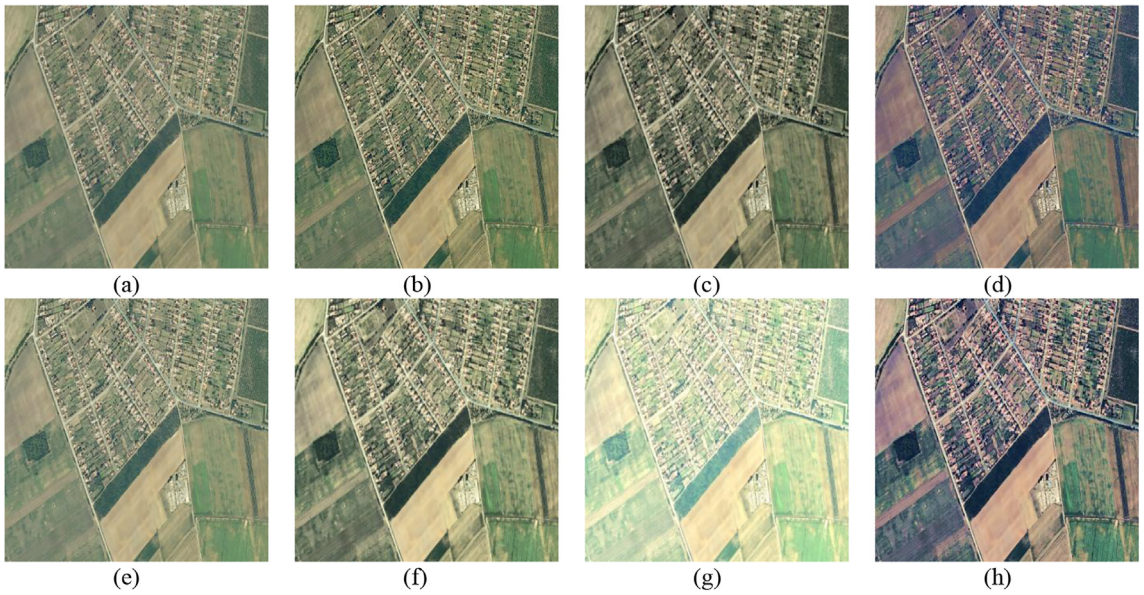

Fig. 10. Visual results of different quality restoration methods for image 7. (a) Original image, (b) UMFKG, (c) RHE-DCT, (d) IFAIR, (e) LSCN, (f) JEI, (g) MDE, (h) PROPOSED FRAMEWORK.

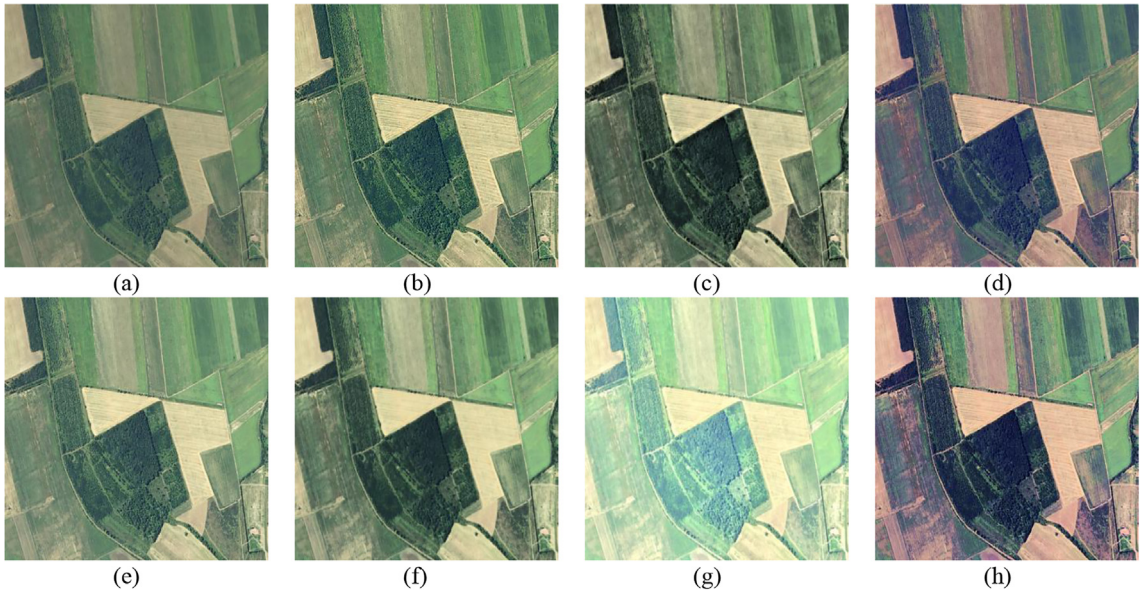

Fig. 11. Visual results of different quality restoration methods for aerial image 8. (a) Original image, (b) UMFKG, (c) RHE-DCT, (d) IFAIR, (e) LSCN, (f) JEI, (g) MDE, (h) PROPOSED FRAMEWORK.

Table 3 and Table 4, it can be seen that performance metrics of proposed framework on aerial image dataset1 and dataset2 are better as compared to other existing image quality restoration methods Performance comparison of difference image quality restoration methods on aerial image dataset1 and dataset2 is also illustrated through bar graph which is shown in Fig. 3.

Further, simulation and experimental quantitative results of the proposed framework is analyzed against other existing image quality restoration methods like UMFKG, RHE-DCT, IFAIR, LSCN, JEI, and MDE on ten aerial images from two aerial image datasets. The visual restoration results of proposed framework and other existing image quality restoration methods are given in Figs. 4–13. From the Figs. 4–13, it can be seen that visual restoration result of UMFKG method does not provide good result. Whereas visual quality restoration results of RHE-DCT method provides better result as compared to UMFKG method but still other details of the image are not very lucid. However, visual quality restoration of IFAIR method provided little improved visual results as compared to UMFKG and RHE-DCT methods but still naturalness is missing in the output image. Further, visual quality restoration of LSCN method provided little improved visual results with cost of information loss at the edges and it also provided faded colors in the output image. The LSCN method also amplifying noisy pixels which introducing small ringing effect because of the use of high pass filter. The visual quality restoration of JEI method has provided better output results but still naturalness is missing in the output image. Whereas, the visual quality restoration of MDE method provided an unnatural output image. Therefore, based on the simulation and experimental results comparison with the other existing image quality restoration methods, the proposed framework has provided better visual and quantitative results.

Fig. 12. Visual results of different quality restoration methods for image 9. (a) Original image, (b) UMFKG, (c) RHE-DCT, (d) IFAIR, (e) LSCN, (f) JEI, (g) MDE, (h) PROPOSED FRAMEWORK.

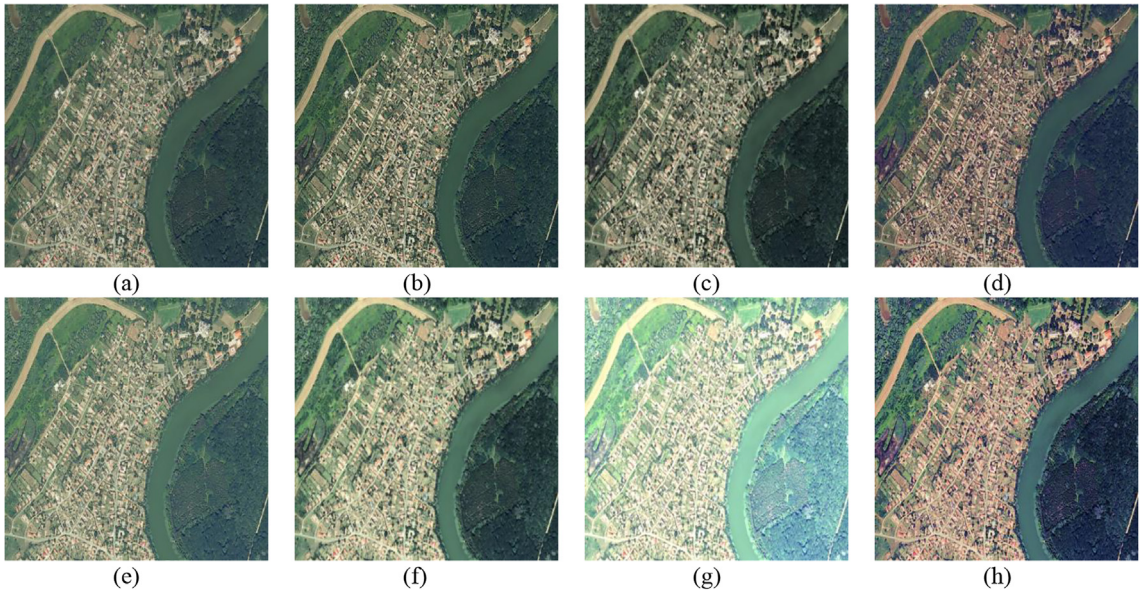

Fig. 13. Visual results of different quality restoration methods for aerial image 10. (a) Original image, (b) UMFKG, (c) RHE-DCT, (d) IFAIR, (e) LSCN, (f) JEI, (g) MDE, (h) PROPOSED FRAMEWORK.

Table 5
CPU processing time of different restoration methods (in second).

Images		Algorithms						
		UMFKG	RHE-DCT	IFAIR	LSCN	JEI	MDE	PROPOSED FRAMEWORK
dataset 1	Image1	18.972	2.806	2.301	9.37	3.306	2816.054	8.071
	Image2	17.997	2.227	2.727	9.333	3.179	2811.022	7.917
	Image3	19.474	1.184	2.128	1.781	0.795	725.160	7.759
	Image4	18.864	2.017	2.262	7.065	2.977	2613.658	7.802
	Image5	19.172	2.208	3.020	14.008	2.971	2447.213	7.788
	Image6	18.729	2.748	2.024	11.762	4.044	945.344	7.342
dataset 2	Image7	17.526	2.077	2.001	14.359	2.698	2425.798	7.042
	Image8	17.548	2.037	1.768	11.254	2.140	2818.628	7.391
	Image9	17.566	1.997	1.972	14.432	2.238	1994.598	7.039
	Image10	17.495	2.023	2.050	14.501	2.088	716.699	7.507

4. Comparison of computational complexity

The CPU processing time for existing image quality restoration methods is presented in Table 5. From the Table 5, it is clear that proposed framework requires slightly higher processing time as compared to RHE-DCT, IFAIR and JEI and lower processing time as compared to UMFKG and MDE. From the Table 5, it is clear that RHE-DCT method takes less processing time as compared to other quality restoration methods because it is based on histogram. From the Table 5, it is also clear that *meta*-heuristic optimization based MDE algorithm takes highest processing time as compared to other existing image quality restoration methods. All the quality restoration methods are implemented in MATLAB R2015a running on an Intel Core i5 - 4210U Laptop with 1.7-GHz CPU, 8-GB RAM, and 64-bit operating system.

5. Conclusion

This paper highlighted proposed framework for contrast enhancement of aerial images. To demonstrate the effectiveness of the proposed framework, the different performance quality parameters were evaluated on different aerial image datasets. The simulation and experimental results were also evaluated and compared with other existing image quality restoration methods. Based on experimental resulted conducted on various aerial images datasets suggested that proposed restoration framework provided better numerical value of NIQMC, BIQME, MICHELSON, DE, EME and PIXDIST as compared to other state-of-the-art quality restoration methods. Visual enhancement results comparison proved that the proposed framework provided better quality restoration results as compared to other state-of-the-art enhancement methods. Comparison of CPU processing time also revealed that the proposed restoration framework was computationally efficient as compared evolutionary based enhancement algorithms such as UMFKG and MDE algorithms. Hence, proposed restoration framework can be used in the pre-processing stage of various applications of image processing. In future work, more efficient nature inspired optimization algorithm could be employed for optimizing parameters.

6. Conflict of interest

There is no conflict of interest.

Appendix A. Supplementary material

Supplementary data associated with this article can be found, in the online version, at https://doi.org/10.1016/j.infrared.2018.08.014.

References

[1] G. Cheng, J. Han, L. Guo, Z. Liu, S. Bu, J. Ren, Effective and efficient midlevel visual elements-oriented land-use classification using VHR remote sensing images, IEEE Trans. Geosci. Remote Sens. 53 (8) (2015) 4238–4249.

[2] Zhu Xijun, L. Guifei, The study of island remote sensing image enhancement, in: First ACIS international symposium on cryptography, and network security, data mining and knowledge discovery, e-commerce and its applications, and embedded systems, pp. 289–291, 2010.

[3] N. Kwok, H. Shi, In Proceedings - International Conference on Machine Learning and Cybernetics, 2015, pp. 322–327, , https://doi.org/10.1109/ICMLC.2015.7340942.

[4] N. Unaldi, S. Temel, K. Vijayan, Asari, Zia-ur Rahman, An automatic wavelet-based nonlinear image enhancement technique for aerial imagery, In: 4th International Conference on Recent Advances in Space Technologies (RAST '09), 1–13 June 2009. pp. 307–382. Doi: 10.1109/RAST.2009.5158217.

[5] S.K. Shen, Jakkula, Aerial image enhancement based on estimation of atmospheric effects, in: Image Processing 2007. ICIP 2007. IEEE International Conference, IEEE, vol. 3, pp. III-529, 2007.

[6] G. Ma, Q. Wei, H. Sui, Q. Qin, Method for large-area satellite image quality enhancement with local aerial images based on non-target multi-point calibration, IEEE J. Sel. Top. Appl. Earth Observ. Remote Sens. 6 (5) (2013) 2174–2183.

[7] T. Arici, S. Dikbas, Y. Altunbasak, A histogram modification framework and its application for image contrast enhancement, IEEE Trans. Image Process. 18 (9) (2003) 706.

[8] D. Sen, S.K. Pal, Automatic exact histogram specification for image contrast enhancement, and visual system based quantitative evaluation, IEEE Trans. Image Process. 20 (5) (2011) 1211.

[9] X. Wu, A linear programming approach for optimal contrast-tone mapping, IEEE Trans. Image Process. 20 (5) (2011) 1262.

[10] T. Celik, T. Tjahjadi, Automatic image equalization and contrast enhancement using Gaussian Mixture modeling, IEEE Trans. Image Process. 21 (1) (2012) 145.

[11] H. Xu, G. Zhai, X. Wu, X. Yang, Generalized equalization model for image enhancement, IEEE Trans. Multimedia 16 (1) (2014) 68.

[12] J. Starck, F. Murtagh, E.J. Candea, D.L. Donoho, Gray and color image contrast enhancement by curvelet transform, IEEE Trans. Image Process. 12 (6) (2003) 706.

[13] J. Tang, J. Kim, E. Peli, Image enhancement in the JPEG domain for people with vision impairment, IEEE Trans. Biomed. Eng. 51 (11) (2004) 2013.

[14] J. Mukherjee, S. Mitra, K: Enhancement of color images by scaling the DCT coefficients, IEEE Trans. Image Process. 17 (10) (2008) 1783.

[15] K. Zhan, J. Shia, J. Teng, Q. Li, M. Wang, F. Lu, Linking synaptic computation for image enhancement, Neurocomputing 238 (2017) 1–12.

[16] X. Fu, J. Wang, D. Zeng, Y. Huang, X. Ding, Remote sensing image enhancement using regularized-histogram equalization and DCT, IEEE Geosci. Remote Sens. Lett. 12 (11) (2015) 2301–2305.

[17] L. Li, Y. Si, Z. Jia, Remote sensing image enhancement based on non-local means filter in NSCT domain, Algorithms 10 (116) (2017) 1–13.

[18] S.K. Pal, D. Bhandari, M.K. Kundu, Genetic algorithms for optimal image enhancement, Pattern Recogn. Lett. 15 (3) (1994) 261–271.

[19] M. Braik, A.F. Sheta, A. Ayesh, Image enhancement using particle swarm optimization, in: the World Congress on Engineering, vol. 1, 2007, pp. 978–988.

[20] A. Gorai, A. Ghosh, Gray-level image enhancement by particle swarm optimization. In: the World Congress on Nature & Biologically Inspired Computing, NaBIC 2009, IEEE, 2009, pp. 72–77.

[21] A. Gorai, A. Ghosh, Hue-preserving color image enhancement using particle swarm optimization, in: IEEE Recent Advances in Intelligent Computational Systems (RAICS), IEEE, 2011, pp. 563–568.

[22] N.M. Kwok, Q.P. Ha, D. Liu, G. Fang, Contrast enhancement and intensity preservation for gray-level images using multiobjective particle swarm optimization, IEEE Trans. Autom. Sci. Eng. 6 (1) (2009) 145–155.

[23] P. Shanmugavadivu, K. Balasubramanian, Particle swarm optimized multi-objective histogram equalization for image enhancement, Opt. Laser Technol. 57 (2014) 243–251.

[24] P. Hoseini, M.G. Shayesteh, Efficient contrast enhancement of images using hybrid ant colony optimisation genetic algorithm and simulated annealing, Digit Signal Process 23 (3) (2013) 879–893.

[25] A. Gogna, A. Tayal, Metaheuristics: Review and application, J. Exp. Theor. Artif. Intell. 25 (4) (2013) 503–526.

[26] P.K. Mahapatra, S. Ganguli, A. Kumar, A hybrid particle swarm optimization and artificial immune system algorithm for image enhancement, Soft. Comput. 19 (8) (2015) 2101–2109.

[27] S. Suresh, S. Lal, Modified differential evolution algorithm for contrast and brightness enhancement of satellite images, Appl Soft Comp 61 (2017) 622–641.

[28] J. Kennedy, R.C. Eberhart, Particle swarm optimization, in: Proc of IEEE International Conference on Neural Networks, Piscataway, NJ, pp. 1942–1948, 1995.

[29] X.S. Yang, Swarm intelligence based algorithms: a critical analysis, Evolut Intell 7 (1) (2014) 17–28.

[30] M. Jmal, W. Souidene, R. Attia, Efficient Cultural heritage image restoration with nonuniform illumination enhancement, J. Electron. Imaging 26 (1) (2017) 011020 011020.

[31] N.M. Kwok, H. Shi, Design of unsharp masking filter kernel and gain using particle swarm optimization, Image and Signal Processing (CISP), in: 7th international Congress, IEEE, pp. 217–222, 2014.

[32] N.M Kwok, H.Y Shi, G. Fang, Q.P. Ha, Intensity-based gain adaptive unsharp masking for image contrast enhancement, Image and Signal Processing (CISP), in: 5th International Congress, IEEE, pp. 529–533, 2012.

[33] S.R.J. Mohamed, S. Rojan Priya, S.Y. Arafath, Particle swarm based unsharp masking, Seventh Indian Conference on Computer Vision, Graphics and Image Processing. pp. 498–505. 2010.

[34] C.L.D.A. Mai, M.T.T. Nguyen, N.M. Kwok, A modified unsharp masking method using particle swarm optimization, in: 4th International Congress on Image and Signal Processing, CISP , vol. 2, pp. 646–650, 2011.

[35] B. Pan, Z. Shi, X. Xu, MugNet: deep learning for hyperspectral image classification using limited samples, ISPRS J. Photogramm. Remote Sens. (2018), https://doi.org/10.1016/j.isprsjprs.2017.11.003.

[36] X. Xu, Z. Shi, B. Pan, ℓ0-based sparse hyperspectral unmixing using spectral information and a multi-objectives formulation, ISPRS J. Photogramm. Remote Sens. 141 (2018) 46–58.

[37] Y. Ren, H. Qi, Q. Chen, L. Ruan, H. Tan, Simultaneous retrieval of the complex refractive index and particle size distribution, Opt Expr 23 (15) (2015) 19328–19337.

[38] C.S. Benedek, T. Szirányi, Change detection in optical aerial images by a multi-layer conditional mixed markov model, IEEE Trans. Geosci. Remote Sens. 47 (10) (2009) 3416–3430.

[39] C.S. Benedek, T. Szirányi, A Mixed Markov Model for Change Detection in Aerial Photos with Large Time Differences. International Conference on Pattern Recognition (ICPR), Tampa, Florida, USA, December 8-11, 2008.

[40] M. Braik, A. Sheta, A. Ayesh, Particle swarm optimization enhancement approach for improving image quality, Int. J. Innov. Comput. Appl. 1 (2) (2007) 138–145.

[41] X.S. Yang, Nature Inspired Optimization algorithm, firstst ed, Elsevier, 2014.

[42] Y. Delice, Aydoğan, U. Özcan, M.S. İlkay, A modified particle swarm optimization algorithm to mixed-model two-sided assembly line balancing, J. Intell. Manuf. 28 (1) (2017) 23–36.
[43] Faria, J. Soares, Z. Vale, H. Morais, T. Sousa, Modified particle swarm optimization applied to integrated demand response and DG resources scheduling, IEEE Trans. Smart Grid 4 (1) (2013) 606–616.
[44] M. Wan, G. Gua, W. Qian, K. Ren, Q. Chen, X. Maldague, Particle swarm optimization-based local entropy weighted histogram equalization for infrared image enhancement, Infrared Phys. Technol. 91 (2018) 164–181.
[45] M.N. Ab Wahab, S. Nefti-Meziani, A. Atyabi, A comprehensive review of swarm optimization algorithms, PLoS One 10(5): e0122827. http://doi.org:/10.1371/journal.pone.0122827.
[46] K. Gu, W. Lin, G. Zhai, X. Yang, W. Zhang, C.W. Chen, No-reference quality metric of contrast-distorted images based on information maximization, IEEE Trans. Cybernet. (2017), https://doi.org/10.1109/TCYB.2016.2575544.
[47] K. Gu, D. Tao, J. Qiao, W. Lin, Learning a no-reference quality assessment model of enhanced images with big data, IEEE Trans. Neural Netw. Learn. Syst. (2017), https://doi.org/10.1109/TNNLS.2017.2649101.
[48] A. Michelson, Studies in Optics, Courier Corp, New York, NY, USA, 1995.
[49] C.E. Shannon, A mathematical theory of communication, Bell Syst. Tech. J. 27 (3) (Jul. 1948) 379–423.
[50] J. Shin, R.H. Park, Histogram-based locality-preserving contrast enhancement, IEEE Signal Process Lett. 22 (9) (2015) 1293–1296.
[51] S. Suresh, D. Das, S. Lal, D. Gupta, Image quality restoration framework for contrast enhancement of satellite remote sensing images, Remote Sens. Appl.: Soc. Environ. 10 (2018) 104–119.
[52] Z. Chen, B.R. Abidi, D.L. Page, M.A. Abidi, Gray-level grouping (GLG): An automatic method for optimized image contrast enhancement-part I: The basic method, IEEE Trans. Image Process. 15 (8) (Aug. 2006) 2290–2302.
[53] C.S. Benedek, T. Szirányi, A mixed markov model for change detection in aerial photos with large time differences, in: International Conference on Pattern Recognition (ICPR), Tampa, Florida, USA, December 8-11, 2008.